Am J Physiol Renal Physiol 305: F1563–F1573, 2013.
First published October 2, 2013; doi:10.1152/ajprenal.00322.2013.

Elucidation of the distal convoluted tubule transcriptome identifies new candidate genes involved in renal Mg^{2+} handling

Jeroen H. F. de Baaij,[1] Marian J. Groot Koerkamp,[2] Marla Lavrijsen,[2] Femke van Zeeland,[1] Hans Meijer,[1] Frank C. P. Holstege,[2] René J. M. Bindels,[1] and Joost G. J. Hoenderop[1]

[1]*Department of Physiology, Nijmegen Centre for Molecular Life Sciences, Radboud University Nijmegen Medical Centre, Nijmegen, The Netherlands; and* [2]*Molecular Cancer Research, UMC Utrecht, Utrecht, The Netherlands*

Submitted 6 June 2013; accepted in final form 30 September 2013

de Baaij JH, Koerkamp MJ, Lavrijsen M, van Zeeland F, Meijer H, Holstege FC, Bindels RJ, Hoenderop JG. Elucidation of the distal convoluted tubule transcriptome identifies new candidate genes involved in renal Mg^{2+} handling. *Am J Physiol Renal Physiol* 305: F1563–F1573, 2013. First published October 2, 2013; doi:10.1152/ajprenal.00322.2013.—The kidney plays a key role in the maintenance of Mg^{2+} homeostasis. Specifically, the distal convoluted tubule (DCT) is instrumental in the fine-tuning of renal Mg^{2+} handling. In recent years, hereditary Mg^{2+} transport disorders have helped to identify important players in DCT Mg^{2+} homeostasis. Nevertheless, several proteins involved in DCT-mediated Mg^{2+} reabsorption remain to be discovered, and a full expression profile of this complex nephron segment may facilitate the discovery of new Mg^{2+}-related genes. Here, we report Mg^{2+}-sensitive expression of the DCT transcriptome. To this end, transgenic mice expressing enhanced green fluorescent protein under a DCT-specific parvalbumin promoter were subjected to Mg^{2+}-deficient or Mg^{2+}-enriched diets. Subsequently, the Complex Object Parametric Analyzer and Sorter allowed, for the first time, isolation of enhanced green fluorescent protein-positive DCT cells. RNA extracts thereof were analyzed by DNA microarrays comparing high versus low Mg^{2+} to identify Mg^{2+} regulatory genes. Based on statistical significance and a fold change of at least 2, 46 genes showed differential expression. Several known magnesiotropic genes, such as transient receptor potential cation channel, subfamily M, member 6 (*Trpm6*), and *Parvalbumin*, were upregulated under low dietary Mg^{2+}. Moreover, new genes were identified that are potentially involved in renal Mg^{2+} handling. To confirm that the selected candidate genes were regulated by dietary Mg^{2+} availability, the expression levels of solute carrier family 41, member 3 (*Slc41a3*), pterin-4 α-carbinolamine dehydratase/dimerization cofactor of hepatocyte nuclear factor-1α (*Pcbd1*), TBC1 domain family, member 4 (*Tbc1d4*), and uromodulin (*Umod*) were determined by RT-PCR analysis. Indeed, all four genes show significant upregulation in the DCT of mice fed a Mg^{2+}-deficient diet. By elucidating the Mg^{2+}-sensitive DCT transcriptome, new candidate genes in renal Mg^{2+} handling have been identified.

magnesium homeostasis; hypomagnesemia; gene expression microarray; Complex Object Parametric Analyzer and Sorter; distal convoluted tubule

HYPOMAGNESEMIA is a common clinical manifestation associated with type 2 diabetes, hypertension, osteoporosis, tetany, seizures, depression, and the use of a variety of drugs (6, 21). Clinical studies addressing the Mg^{2+} status of critically ill patients showed that a substantial number of patients were hypomagnesemic. Moreover, low blood Mg^{2+} levels are associated with a poor clinical outcome (23, 40). The regulation of blood Mg^{2+} levels is an equilibrium between intestinal Mg^{2+} absorption and renal Mg^{2+} reabsorption. In the kidney, Mg^{2+} reabsorption in the proximal tubule and thick ascending limb of Henle (TAL) is a passive paracellular process, whereas in the distal convoluted tubule (DCT), Mg^{2+} reabsorption is a highly regulated and transcellular mechanism. This latter segment facilitates the fine-tuning of renal Mg^{2+} uptake, since no reabsorption takes places beyond the DCT.

Over the last decade, the elucidation of the molecular origin of human genetic diseases has helped to identify new proteins involved in Mg^{2+} transport in the DCT (6). In patients with hypomagnesemia and secondary hypocalcemia, mutations have been identified in transient receptor potential (TRP) subfamily M, member 6 (*TRPM6*), the gatekeeper of Mg^{2+} entry in DCT cells (39, 47). The abundance of TRPM6 at the plasma membrane is regulated by EGF, and, as a result, mutations in the *pro-EGF* gene are causative for hypomagnesemia (16). Mg^{2+} transport via TRPM6 is a passive process that depends on the membrane potential across the luminal membrane (14). Therefore, several players involved in the maintenance of this membrane potential have been identified by gene-linkage analyses in patients with hereditary hypomagnesemia. For instance, a mutation in *KCNA1*, which encodes the voltage-gated K^+ channel Kv1.1, impairs the luminal extrusion of K^+ necessary to maintain a substantial luminal membrane potential (14). At the basolateral membrane, the K^+ channel Kir4.1 acts an important player in the K^+ recycling that seems necessary to maintain high Na^+-K^+-ATPase activity (1). Indeed, mutations in *KCNJ10*, which codes for Kir4.1, and mutations in *FYXD2*, which codes for the γ-subunit of Na^+-K^+-ATPase, have been linked with hypomagnesemia (1, 4). Moreover, mutations in the transcription factor hepatocyte nuclear factor (HNF)-1β (*HNF1B*), which regulates the transcription of *FXYD2*, cause a similar phenotype (27). Recently, mutations in the DCT-expressed cyclin M2 (*CNNM2*) gene have been linked with hypomagnesemia (43). It was postulated that CNNM2 may act as an intracellular Mg^{2+} sensor regulating Mg^{2+} transport (7). Although gene linkage studies have gained insights into Mg^{2+} reabsorption in the DCT over the last years, several factors remain unidentified. For instance, at present, the Mg^{2+} extrusion mechanism of DCT cells is still unknown.

The aim of the present study was, therefore, to elucidate the Mg^{2+}-sensitive transcriptome of the DCT cell. To this end, primary DCT cells were isolated from mouse kidneys, and a comprehensive expression profile specific for DCT cells was established using gene expression microarrays. Furthermore, by comparing DCT expression profiles of mice fed high and

Address for reprint requests and other correspondence: J. G. J. Hoenderop, Dept. of Physiology (286), Radboud Univ. Nijmegen Medical Centre, Nijmegen Centre for Molecular Life Sciences, PO Box 9101, Nijmegen 6500 HB, The Netherlands (e-mail: J.Hoenderop@fysiol.umcn.nl).

 1931-857X/13 Copyright © 2013 the American Physiological Society

Downloaded from http://ajprenal.physiology.org/ by 10.220.33.6 on October 20, 2016

low Mg^{2+}-containing diets, the Mg^{2+} sensitivity of the DCT transcriptome was determined. Here, we describe the identification of new candidate genes potentially involved in Mg^{2+} reabsorption in the DCT.

MATERIALS AND METHODS

Animal experiments. All the experimental procedures are in compliance with the animal ethics board of Radboud University (Nijmegen, The Netherlands). Transgenic C57Bl/6 mice expressing enhanced green fluorescent protein (eGFP) under the parvalbumin (PV) promotor were kindly provided by Dr. Hannah Monyer (University of Heidelberg, Heidelberg, Germany) (29). The genotype was determined under ultraviolet light by checking the fluorescent emission of muscular PV expression in mouse legs. Littermates were housed in a temperature- and light-controlled room with standard pellet chow (SSNIFF Spezialdiäten, Soest, Germany) and deionized drinking water available ad libitum until the start of the experiment. PV-eGFP-positive mice were selected for experiments at the age of 4–6 wk. During the experiments, mice were fed low [0.02% (wt/wt)] or high [0.48% (wt/wt)] Mg^{2+}-containing diets for 15 days (SSNIFF Spezialdiäten). During the last 48 h of the experiment, mice were housed in metabolic cages for urine and fecal collection (24-h adaptation, 24-h sampling). Blood samples were taken at the start of the experiment and just before euthanization.

Isolation of the DCT using Complex Object Parametric Analyzer and Sorter sorting. PV-eGFP-positive tubules were isolated as previously described (26). In brief, mice aged 4–6 wk were anesthetized and perfused transcardially with ice-cold Krebs buffer [containing (in mM) 145 NaCl, 5 KCl, 1 NaH_2PO_4, 2.5 $CaCl_2$, 1.8 $MgSO_4$, 10 glucose, and 10 HEPES/NaOH; pH 7.4]. Directly after perfusion of the mice, whole kidneys were harvested, and eGFP-positive kidney material was manually selected under a microscope. This part of the procedure took up to 30–45 min. Subsequently, fragments of the kidney were digested in Krebs buffer containing 1 mg/ml collagenase (Worthington, Lakewood, NJ) and 2,000 U/ml hyaluronidase (Sigma, Houten, The Netherlands) for 15 min at 37°C. Subsequently, kidney tubules sized between 40 and 100 μm were collected by filtration. Oversized material was digested again in two additional cycles of 10-min digestion and filtration. Tubules collected from the three digestions were ice cooled and sorted by the Complex Object Parameric Analyzer and Sorter (COPAS; Union Biometrica, Holliston, MA) at a rate of 2,000–4,000 tubules/h. Sorted tubules were directly collected in 1% (vol/vol) β-mercaptoethanol containing RLT buffer supplied by the RNeasy RNA extraction kit (Qiagen, Venlo, The Netherlands). In total, the sorting procedures of tubules from one mouse took several hours. Per mouse, 4,000 eGFP-positive fluorescent tubules were collected, and, as a control, an additional 4,000 tubules were sorted from the same kidney sample without selection for eGFP-positive cells. This control sample contained both eGFP-positive and eGFP-negative cells of the same size as the selected sample. Four thousand ubules were pooled on a Qiagen Rneasy microcolumn for RNA extraction according to the manufacturer's protocol.

Microarray analysis. For microarray experiments, RNA from two male and two female mice per group was taken. RNA from low- and

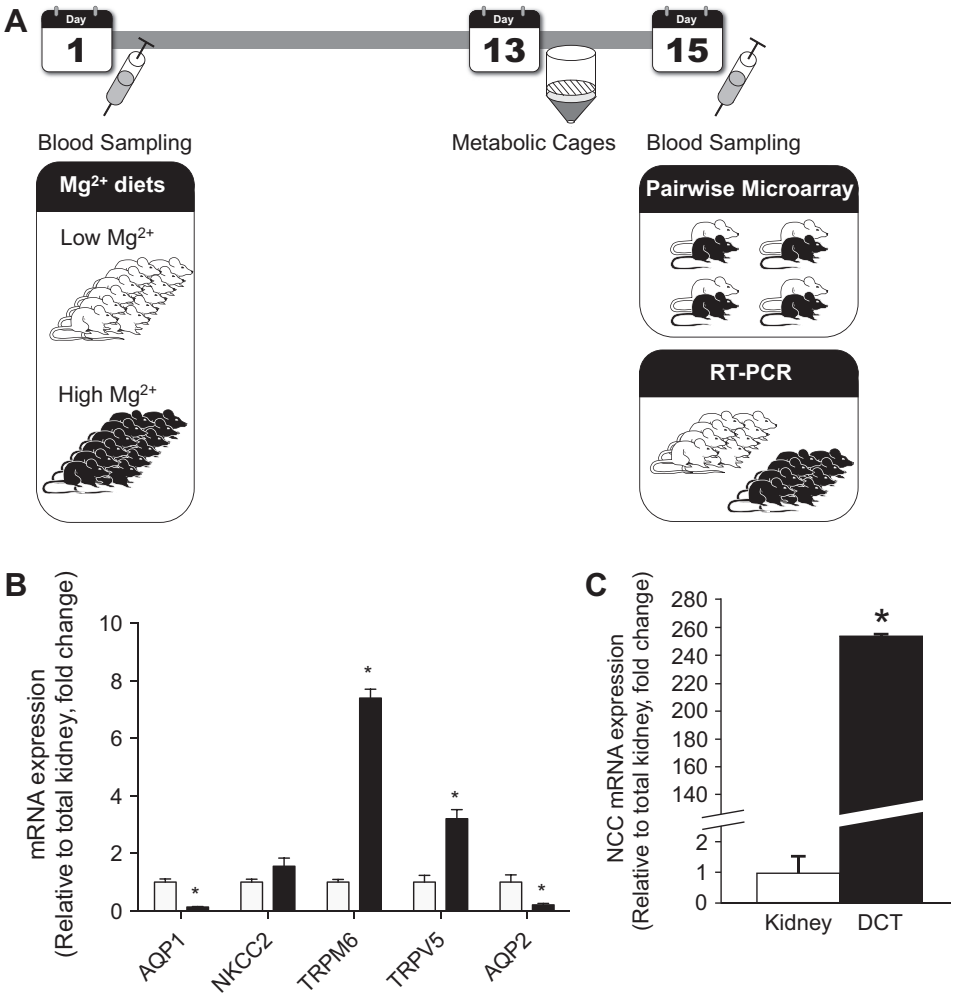

Fig. 1. Isolation of distal convoluted tubule (DCT) cells. *A*: timeline of animal experiments. Mice were placed on Mg^{2+} diets for 15 days (shaded bar). Blood samplings are indicated by needles; metabolic cages are represented by the cage diagram. *B* and *C*: mRNA expression levels of aquaporin 1 (*Aqp1*), Na^+-K^+-2Cl cotransporter 2 (*Nkcc2*), transient receptor potential (TRP) cation channel, subfamily M, member 6 (*Trpm6*), *Trpv5*, and *Aqp2* (*B*) and Na^+-Cl^{-1} cotransporter (*Ncc*; *C*) in Complex Object Parametric Analyzer and Sorter (COPAS)-selected mouse DCT and control (none selected) kidney tubules were measured by quantitative RT-PCR and normalized for Gapdh expression. Data represent means ± SE and are expressed as fold differences compared with the expression in none-selected tubules; $n = 8$. $*P < 0.05$ indicates a significant difference from none-selected tubules.

Downloaded from http://ajprenal.physiology.org/ by 10.220.33.6 on October 20, 2016

high-Mg^{2+} groups was matched in pairs based on the sex of the mice. Double-round RNA amplifications and labeling were performed as previously described (37) on an automated system (Caliper Life Sciences) with 10–50 ng total RNA from each sample. Briefly, total RNA was amplified twice from ~50,000 cells by cDNA synthesis with oligo(dT) double-anchored primers followed by in vitro transcription using a T7 RNA polymerase kit (Ambion, Bleiswijk, The Netherlands). During the second round of transcription, 5-(3-aminoallyl)-UTP was incorporated into the single-stranded cRNA. Cy3 and Cy5 *N*-hydroxysuccinimide esters (Amersham Biosciences, Roosendaal, The Netherlands) were coupled to 2 μg cRNA. RNA quality was monitored after each successive step using the equipment described above. Mouse Whole Genome Gene Expression Microarrays (V2, Agilent Technologies), representing 39,429 *Mus musculus* 60-mer probes in a 4 × 44-K layout, were used for hybridizations with 1 μg of each alternatively labeled cRNA on a HS4800PRO system supplemented with QuadChambers (Tecan Benelux) according to van de Peppel et al. (45). After hybridization, slides were scanned using the Agilent G2565BA DNA Microarray Scanner.

After automated data extraction using Imagene 8.0 software (BioDiscovery), Lowess normalization was performed on mean spot intensities followed by dye bias correction based on a within-set estimate, as previously described (25, 50). Data were analyzed using MAANOVA (49). In a fixed effect analysis, sample, array, and dye effects were modeled. *P* values were determined by a permutation *F*2-test, in which residuals were shuffled 5,000 times globally. Genes with *P* values of <0.05 after family-wise error correction were considered significantly changed. Additionally, a twofold change cutoff was applied.

The complete microarray dataset was deposited in the Gene Expression Omnibus (GEO; http://www.ncbi.nlm.nih.gov/geo/) under Accession Number GSE40208.

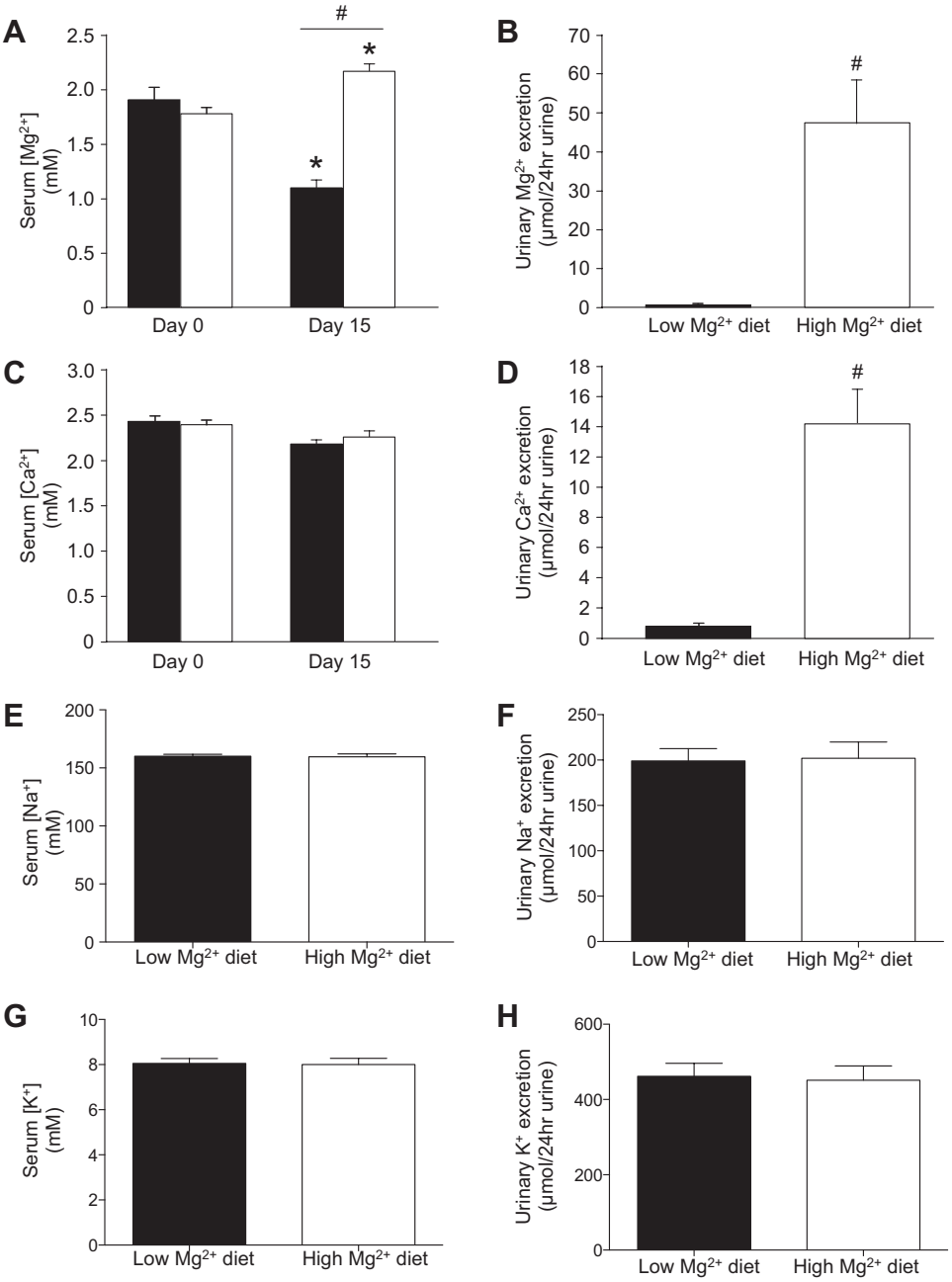

Fig. 2. Effect of the dietary Mg^{2+} availability on serum and urinary Na^+, K^+, Mg^{2+} and Ca^{2+} concentrations. *A* and *C*: serum Mg^{2+} (*A*) and Ca^{2+} (*C*) concentrations at *days 0* and *15* of mice fed a low or high Mg^{2+}-containing diet for 15 days. *B* and *D*: 24-h urinary Mg^{2+} (*B*) and Ca^{2+} (*D*) excretion at *day 15* of mice fed a low or high Mg^{2+}-containing diet for 15 days. *E* and *G*: serum Na^+ (*E*) and K^+ (*G*) concentrations at *day 15* of mice fed a low or high Mg^{2+}-containing diet for 15 days. *F* and *H*: 24-h urinary Na^+ (*F*) and K^+ (*H*) excretion at *day 15* of mice fed a low or high Mg^{2+}-containing diet for 15 days. Values are presented as means ± SE; $n = 12$. *$P < 0.05$ was considered statistically significant compared with *day 0*; #$P < 0.05$ was considered statistically significant to the low-Mg^{2+} group.

Downloaded from http://ajprenal.physiology.org/ by 10.220.33.6 on October 20, 2016

Mg^{2+} and Ca^{2+} analysis. Serum and urine total Mg^{2+} and Ca^{2+} concentrations were determined using a colorimetric assay kit according to the manufacturer's protocol (Roche Diagnostics, Woerden, The Netherlands). Urine volume was measured to calculate 24-h Mg^{2+} excretion.

Quantitative real-time PCR. The obtained mRNA from 4,000 tubules was reverse transribed using Moloney murine leukemia virus reverse transcriptase (Invitrogen, Bleiswijk, The Netherlands) for 1 h at 37°C. cDNA was subsequently used to measure PV, Na^+-Cl^- cotransporter (*Ncc*), *Trpm6*, *Kcna1*, *Kcnj10*, *Egf*, *Fxyd2*, *Hnf1b*, *Cnnm2*, solute carrier family 41, member 3 (*Slc41a3*), pterin-4 α-carbinolamine dehydratase/dimerization cofactor of HNF-1α (*Pcbd1*), TBC1 domain family, member 4 (*Tbc1d4*), and uromodulin (*Umod*) mRNA levels. Gene expression levels were determined by quantitative real-time PCR on a Bio-Rad analyzer and normalized for *Gapdh* expression. Primer sequences are shown in Supplemental Table S2.[1]

Immunohistochemistry. Immunohistochemistry was performed as previously described (13). In brief, costaining for UMOD with thiazide-sensitive NCC was performed on 5-μm sections of fixed frozen mouse kidney samples. Sections were incubated for 16 h at 4°C with the following primary antibodies: guinea pig anti-UMOD (1:750, BioTrend, Köln, Germany) and rabbit anti-NCC [1:100 (32)]. For detection, kidney sections were incubated with Alexa fluor-conjugated secondary antibodies. Images were taken with an AxioCam camera and AxioVision software (Zeiss, Sliedrecht, The Netherlands).

Statistical analysis. For RT-PCR experiments, statistical significance was determined using an unpaired Student's *t*-test. In all experiments, data are expressed as means ± SE. Differences with *P* values of <0.05 were regarded as statistically significant.

RESULTS

Experimental design. In our study, transgenic mice expressed eGFP downstream of a PV promoter were subjected to Mg^{2+} diets. Within the kidney, PV is exclusively expressed in the DCT (3). Combining PV-eGFP mice with the COPAS tissue sorting system allowed the specific isolation of DCT cells (26). Here, PV-eGFP mice were subdivided into 2 groups consisting of 12 mice each. Each group was subjected to a high [0.48% (wt/wt)] or low [0.02% (wt/wt)] Mg^{2+}-containing diet for 15 days. Subsequently, DCT tubules were isolated using COPAS, and total RNA was extracted (Fig. 1*A*). Four of twelve pairs of RNA extracts were processed for and subjected to pairwise (high vs. low) microarray analysis. The eight remaining RNA extracts per group were used to validate the results of the microarray experiments by RT-PCR.

As a control for purity, transcriptional expression levels of the DCT marker genes *Trpm6* and *Ncc* were determined by RT-PCR (Fig. 1, *B* and *C*). Indeed, expression of thiazide-sensitive *Ncc* and *Trpm6* were enriched by 200- and 8-fold, respectively, compared with total kidney material of the same mice. Moreover, expression of the protein markers for proximal tubules [aquaporin 1 (*Aqp1*)] and the collecting duct (*Aqp2*) was reduced. A slight overlap was detected with the TAL and connecting tubules when samples were tested for the marker genes Na^+-K^+-2Cl cotransporter 2 (*Nkcc2*) and *Trpv5*, respectively (Fig. 1*B*). These results indicate that the COPAS-sorted tubules contained primarily DCT transcripts.

Effects of Mg^{2+} diets. Before mRNA transcripts were subjected to microarray hybridization, the effects of Mg^{2+} diets on plasma and urinary Mg^{2+} levels were assessed (Fig. 2, *A–C*). In line with our previous experiments, the serum Mg^{2+} concentration dropped significantly in mice fed the Mg^{2+}-deficient diet (Fig. 2*A*) (15). The Mg^{2+}-enriched diet resulted in slight, albeit significant, hypermagnesemia (Fig. 2*A*). Urinary Mg^{2+} excretion showed the same pattern: high excretion in mice fed the Mg^{2+}-enriched diet and low excretion in mice fed the Mg^{2+}-deficient diet (Fig. 2*B*). Serum Ca^{2+} concentrations did not change significantly (Fig. 2*C*). In contrast, the urinary Ca^{2+} concentration was significantly increased in mice fed a high-Mg^{2+} diet (Fig. 2*D*). Urinary and serum Na^+ and K^+ values were not significantly altered by dietary Mg^{2+} availability (Fig. 2, *E–H*).

DCT transcriptome analysis. The DCT transcriptome was first analyzed for abundance of individual mRNAs. This was achieved by analyzing the average $\log_2$ intensity of the two-channel microarray data [the so-called "*A* value", where $A = ½\log_2(RG)$] after normalization between the two channels. Although the *A* value is influenced by the amplification of the transcripts and the position of microarray feature sequences, it gives a qualitative view of the gene expression level in DCT tubules. Of the most abundant transcripts, more than one-third were directly linked to mitochondrial function (see Supplemental Table S1). The DCT cells are the cells with the highest mitochondrial density in the mammalian kidney (9). Moreover, DCT marker genes have moderate to high *A* values. *Ncc* gave an average expression signal of 11.9, and *Trpm6* had a value of 11.7. Several genes implicated in DCT-mediated Mg^{2+} transport were highly expressed. *Egf* and *Fxyd2* were among the 50 most expressed DCT genes, with expression values of 16.7 and 16.5. Interestingly, marker proteins of the TAL showed low expression levels. For instance, *Nkcc2* had a value of 8.6 and *Claudin16* had an expression level of 6.9. Taken together, these results confirm the purity of the COPAS-selected DCT cells.

Mg^{2+}-sensitive gene expression. To identify the DCT genes involved in Mg^{2+} homeostasis, Mg^{2+}-sensitive differential

Table 1. *Mg^{2+} sensitivity in the DCT of genes associated with hypomagnesemia*

Name	Average Signal (*A* Value)	Fold Change in the Low-Mg^{2+} Group	*P* Value
Trpm6	11.8	2.05	0.03
Egf	16.7	1.74	0.05
Kcna1	5.7	0.97	1
Kcnj10	14.9	1.08	1
Fxyd2	16.5	0.88	1
Hnf1b	8.7	0.84	1
Cnnm2	10.4	1.69	0.68
Slc12a3	11.9	1.11	1

Shown is a summary of Mg^{2+}-sensitive expression of all distal convoluted tubule (DCT) genes previously linked with human genetic forms of hypomagnesemia by microarray expression analysis on mRNA specifically isolated from DCT material. The average signal is expressed as the $\log_2$ of the sum of the red and green signal divided by 2. The fold change is the differential expression between high- and low-Mg^{2+} diet-fed mice and is expressed as enrichment in the low-Mg^{2+} diet compared with the high-Mg^{2+} diet. Numbers above 1 indicate enrichment in mice fed a low-Mg^{2+} diet. Numbers below 1 designate enrichment in mice fed with high-Mg^{2+} diet. The *P* value shows the statistical significance of the differential expression. *Trpm6*, transient receptor potential cation channel, subfamily M, member 6; *Kcna1*, K^+ voltage-gated channel, shaker-related subfamily, member 1; *Kcnj10*, K^+ inwardly rectifying channel, subfamily J, member 10; *Fxyd2*, FXYD domain containing ion transport regulator 2; *Hnf1b*, hepatocyte nuclear factor-1β; *Cnnm2*, cyclin M2; *Slc12a3*, solute carrier family 12, member 3.

[1] Supplemental Material for this article is available at the *American Journal of Physiology-Renal Physiology* website.

Downloaded from http://ajprenal.physiology.org/ by 10.220.33.6 on October 20, 2016

expression of the transcriptome was determined by pair-wise comparison of high versus low Mg^{2+} samples. As a first approach, we examined the expression of the genes that are associated with hypomagnesemia in genetic disease (6). Interestingly, only *Trpm6* and *Egf* were shown to be significantly upregulated in mice fed the low-Mg^{2+} diet compared with mice fed with the high-Mg^{2+} diet (Table 1). To assess the reproducibility of our microarray data, the microarray results were validated by RT-PCR on a separate set of DCT mRNA transcripts (Fig. 3, *A–H*). Indeed, this analysis confirmed that dietary Mg^{2+} regulates *Trpm6* expression. *Trpm6* expression in low-Mg^{2+} diet-fed mice was 2.3-fold enriched compared with mice fed the high-Mg^{2+} diet (Fig. 3*A*). Additionally, only *Egf* and *Cnnm2* were differentially regulated (Fig. 3, *B* and *F*). RT-PCR analyses showed enrichment in low-Mg^{2+} diet-fed mice of 1.5- and 2.1-fold, respectively, relatively to high-Mg^{2+} diet-fed mice. The enrichment of *Cnnm2* was not significant in the microarray data ($P = 0.68$) but was highly significant in the RT-PCR analysis ($P < 0.002$). *Kcna1* transcripts, which encode Kv1.1, were not detectable in the pure DCT material (Fig. 3*C*), confirming the low signal in the microarray (*A* value: 5.7). No major differences between microarray and RT-PCR data were observed, indicating high reproducibility between the RT-PCR and microarray analyses.

Next, we analyzed the microarray Mg^{2+} sensitivity of all potential mammalian Mg^{2+} transporters that have been described in the literature (34). Compared with mice fed a Mg^{2+}-enriched diet, only *Trpm6* and *Slc41a3* mRNA transcripts showed a significant enrichment in mice fed a Mg^{2+}-deficient diet (Table 2). *Slc41a3* has been previously linked to Mg^{2+} transport, although the exact function of this gene was never examined (34). *Cnnm1*, *Cnnm3*, *Cnnm4*, *Slc41a1*, and *Slc41a2* and all other transporters of the NaCl-inducible protein (*Nipa*), *MagT*, membrane Mg^{2+} transporter (*MMgT*), *Mrs*, and putative ZDHHC-type palmitoyltransferase 6-like (*Zdhhc*) families are not Mg^{2+} sensitive and presented relatively low *A* values, suggesting low DCT abundance.

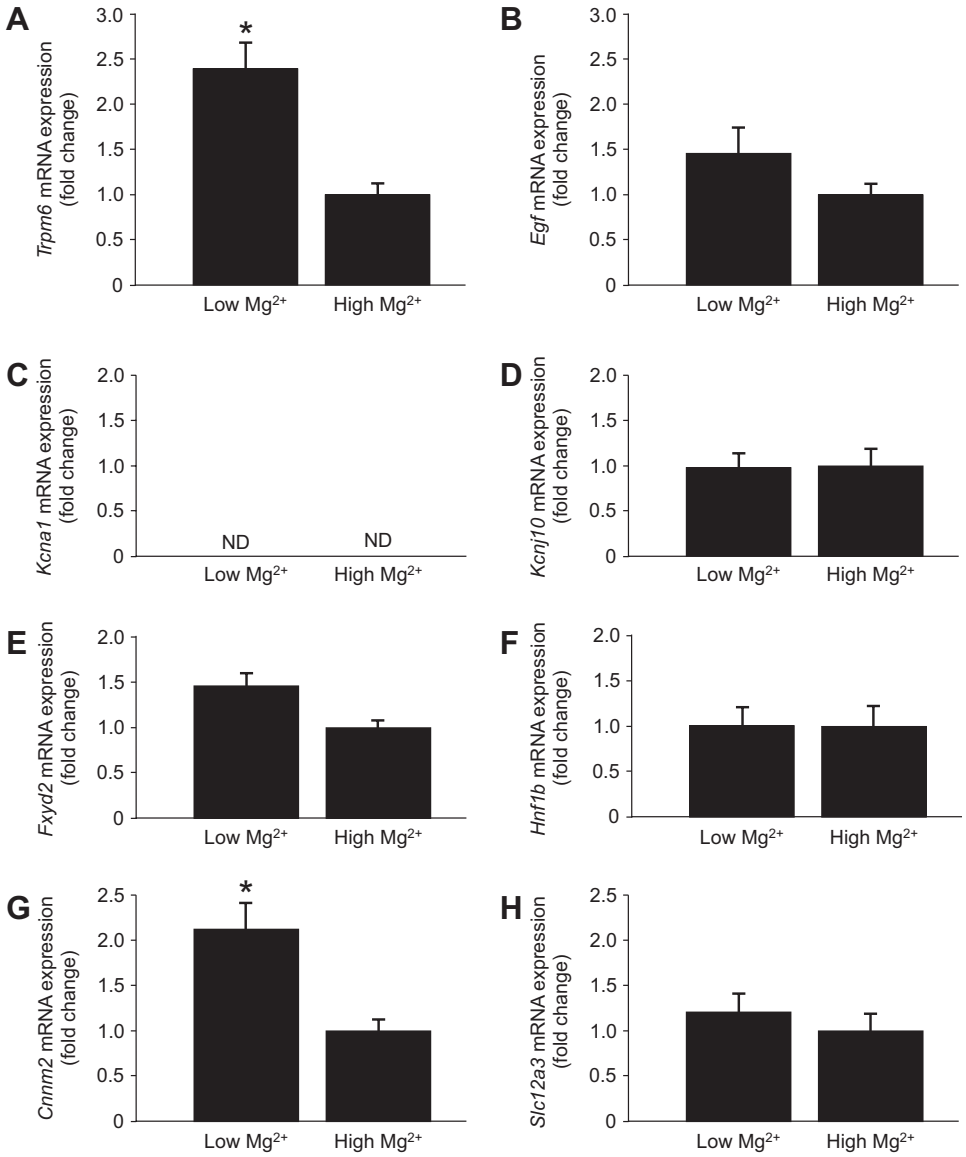

Fig. 3. Effects of dietary Mg^{2+} availability on mRNA transcript expression of hypomagnesemia-linked genes. *A–H*: mRNA expression levels of *Trpm6* (*A*), *Egf* (*B*), K^+ voltage-gated channel, shaker-related subfamily, member 1 (*kcna1*; *C*), K^+ inwardly rectifying channel, subfamily J, member 10 (*Kcnj10*; *D*), FXYD domain containing ion transport regulator 2 (*Fxyd2*; *E*), hepatocyte nuclear factor-1β (*Hnf1b*; *F*), cyclin M2 (*Cnnm2*; *G*) and Ncc (*H*) in COPAS-selected DCT tubules of mice fed a low or high Mg^{2+}-containing diet for 15 days were measured by quantitative RT-PCR and normalized for *Gapdh* expression. Data represent means ± SE and are expressed fold differences compared with expression in the high-Mg^{2+} group; $n = 8$. ND, not detectable. $*P < 0.05$ indicates a significant difference from the high-Mg^{2+} group.

Downloaded from http://ajprenal.physiology.org/ by 10.220.33.6 on October 20, 2016

Table 2. *Mg^{2+}-sensitivity in the DCT of Mg^{2+} transporters*

Name	Average Signal (*A* Value)	Fold Change in the Low-Mg^{2+} Group	*P* Value
Trpm6	11.8	2.05	0.03
Trpm7	14.3	1.37	0.49
Cnnm1	8.4	0.86	1
Cnnm2	13.5	1.69	0.68
Cnnm3	11.5	1.21	1
Cnnm4	7.1	0.95	1
Slc41a1	6.8	1.03	1
Slc41a2	5.6	0.99	1
Slc41a3	7.8	2.02	0.02
Nipa1	8.6	0.98	1
Nipa2	9.9	1.15	1
Nipal1	5.9	1.01	1
Nipal2	5.8	0.94	1
Nipal3	11.8	1.09	1
Nipal4	5.1	1.00	1
Mrs2	8.3	0.75	1
MagT1	7.8	0.98	1
MMgT1	7.8	1.06	1
MMgT2	8.3	1.29	1
Tusc3	8.7	0.98	1
Zdhhc17	7.9	1.20	1
Zdhhc13	8.5	1.05	1

Shown is Mg^{2+}-sensitive expression of all putative mammalian Mg^{2+} transporters by microarray expression analysis on mRNA specifically isolated from DCT material. The average signal is expressed as the $\log_2$ of the sum of the red and green signal divided by 2. The fold change is the differential expression between high- and low-Mg^{2+} diet-fed mice and is expressed as enrichment in the low-Mg^{2+} diet compared with the high-Mg^{2+} diet. Numbers above 1 indicate enrichment in mice fed with a low-Mg^{2+} diet. Numbers below 1 designate enrichment in mice fed with a high-Mg^{2+} diet. The *P* value shows the statistical significance of the differential expression. *Nipa*, NaCl-inducible protein; *MMgT*, membrane Mg^{2+} transporter; *Tusc3*, tumor suppressor candidate 3; *Zdhhc*, putative ZDHHC-type palmitoyltransferase 6-like.

New candidate genes. The main objective of this study was to identify new players in renal Mg^{2+} handling. Therefore, we subsequently selected differentially expressed genes with statistical significance ($P < 0.05$) and a minimal fold change in expression of two. As a result of this stringent analysis, 46 gene candidates were identified (Table 3). Among the genes that were enriched in Mg^{2+}-deficient mice, previously mentioned *Trpm6* and *Slc41a3* were detected. Additionally, 33 genes were identified that were enriched in the low-Mg^{2+} group (compared with the high-Mg^{2+} group). The gene with the highest fold change was sex-determining region Y-box 9 (*Sox9*), which encodes a transcription factor involved in renal development. Other high-ranking genes were the DCT marker *Pv*, glycoprotein *Umod*, and complement factor *Cd55*. Furthermore, we identified direct and indirect regulators of Na^+-K^+-ATPase, *Tbc1d4* and *Pcbd1*. Notable was the presence of several genes that are mainly known for their role in Ca^{2+} homeostasis, such as calbindin$_{28K}$ (*Calb1*) and the vitamin D receptor (*Vdr*). Only 11 genes were significantly enriched with a minimal fold change of two in the high-Mg^{2+} group compared with the low-Mg^{2+} group. None of these genes were previously linked to Mg^{2+} homeostasis. The most profound differential expression was measured with the PGE receptor 3 (subtype EP_3) gene (*Ptger3*), which encodes a prostaglandin receptor.

To confirm the results of the microarray analysis, mRNA transcript levels of all major candidate genes were determined using RT-PCR (Fig. 4, *A–D*). Indeed, *Slc41a3* mRNA expression was 1.8-fold enriched in Mg^{2+}-deficient mice, similar to the values observed on the microarray (Fig. 4*A*). Likewise, mRNA expression levels were determined for *Pcbd1*, *Tbc1d4*, and *Umod*, since all three genes are potentially involved in Mg^{2+} handling (Fig. 4, *B–D*). Pcbd1 is a regulator of HNF-1β function, Tbc1d4 has been shown to modulate Na^+-K^+-ATPase activity, and Umod effects transcellular Na^+ transport (2, 28, 31). The fold enrichment values for

Table 3. *Mg^{2+}-regulated genes in the DCT*

Name	Average Signal (*A* Value)	Fold Change in the Low-Mg^{2+} Group	*P* Value
Sox9	9.6	4.83	0.01
Cd55	7.1	4.16	0.00
Dnaja4	11.8	3.28	0.00
Gulo	8.4	3.27	0.02
Pck1	9.0	3.27	0.03
Prkd1	9.7	3.17	0.0004
Calb1	13.5	3.01	0.02
Umod	16.3	2.91	0.01
Pvalb	13.4	2.71	0.01
Ptgs1	10.0	2.52	0.0008
Tppp	6.4	2.52	0.01
Unc5b	10.6	2.37	0.00
Rd3	9.5	2.36	0.01
Acss1	15.7	2.30	0.03
Wdr72	11.8	2.27	0.02
Pdlim1	7.8	2.20	0.03
Pcbd1	14.8	2.20	0.01
Tbc1d4	11.6	2.18	0.01
Gsn	12.8	2.17	0.02
Ilvbl	8.2	2.12	0.01
Spag5	6.5	2.12	0.03
Etv5	10.3	2.11	0.01
Vdr	10.7	2.10	0.01
Hmgcll1	8.1	2.09	0.0012
Iyd	7.4	2.08	0.03
Zscan4c	9.4	2.08	0.02
Plekha1	12.0	2.08	0.0018
Trpm6	11.8	2.05	0.03
Tspan33	10.8	2.04	0.01
Abcg1	8.1	2.04	0.02
Dusp6	10.6	2.03	0.02
Gpm6b	8.7	2.02	0.01
Slc41a3	7.8	2.02	0.02
Cwh43	13.3	2.01	0.03
Tdrd3	12.9	2.00	0.0008
Pdpn	9.0	0.49	0.002
Gpc3	7.0	0.49	0.02
Lrtm2	8.3	0.48	0.05
Nqo1	8.3	0.46	0.03
Tmed6	8.7	0.45	0.0004
Grin3a	6.8	0.44	0.01
Ell3	8.3	0.42	0.00
Kap	9.2	0.40	0.01
Mreg	9.6	0.38	0.00
Ndrg4	9.1	0.37	0.01
Ptger3	9.5	0.23	0.01

Shown is a summary of all genes that were significantly ($P < 0.05$) differentially expressed with a minimal fold change of two in the DCT of mice fed with a high or low Mg^{2+} diet for 15 days, as determined by microarray expression analysis on mRNA specifically isolated from DCT material. The average signal is expressed as the $\log_2$ of the sum of the red and green signal divided by 2. The fold change is the differential expression between high- and low-Mg^{2+} diet-fed mice and is expressed as enrichment in the low-Mg^{2+} diet compared with the high-Mg^{2+} diet. Numbers above 1 indicate enrichment in mice fed a low-Mg^{2+} diet. Numbers below 1 designate enrichment in mice fed a high-Mg^{2+} diet. The *P* value shows the statistical significance of the differential expression. The full list of 35,000 genes can be accessed at the Gene Expression Omnibus database under Accession no. GSE40208.

Downloaded from http://ajprenal.physiology.org/ by 10.220.33.6 on October 20, 2016

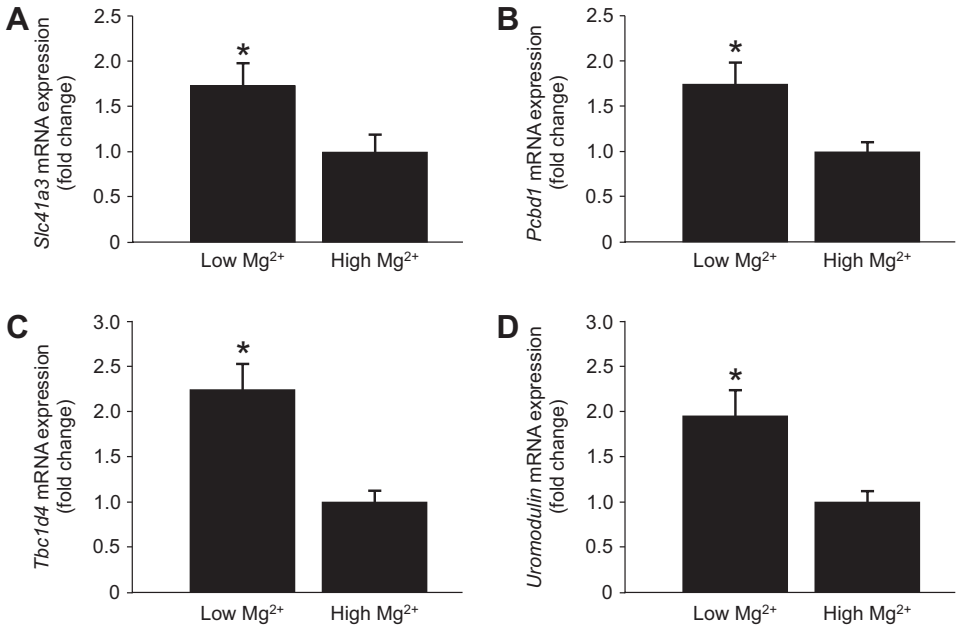

Fig. 4. Effects of dietary Mg^{2+} availability on mRNA transcript expression of newly identified candidate genes. *A–D*: the mRNA expression levels of solute carrier family 41, member 3 (*Slc41a3*; *A*), pterin-4 α-carbinolamine dehydratase/dimerization cofactor of HNF-1α (*Pcbd1*; *B*), TBC1 domain family, member 4 (*Tbc1d4*; *C*), and uromodulin (*Umod*; *D*) in COPAS-selected DCT tubules of mice fed a low or high Mg^{2+}-containing diet were measured by quantitative RT-PCR and normalized for *Gapdh* expression. Data represent means ± SE and are expressed fold differences compared with expression in the high-Mg^{2+} group; $n = 8$. $*P < 0.05$ indicates a significant difference from the high-Mg^{2+} group.

these three genes estimated by RT-PCR corresponded with the values obtained by the microarray analysis. Since *Umod* is mainly described as a TAL gene, we further examined *Umod* DCT expression with immunohistological staining and RT-PCR. Interestingly, *Umod* was 3.5 times more expressed in DCT cells compared with total kidney material (Fig. 5*A*). UMOD colocalized with NCC in early DCT cells (Fig. 5*C*). Moreover, only the DCT fraction of *Umod* expression, but not the total kidney sample mainly containing TAL *Umod* expression, was shown to be Mg^{2+} sensitive (Fig. 5*B*).

To determine whether the differentially regulated genes belong to the same functional pathways or cellular processes, Gene Oncology (GO) term enrichment analysis was performed by gene set enrichment analysis (Table 4). In DCT samples from Mg^{2+}-deficient mice, EGF signaling was upregulated, as evidenced by the differentially regulated GO term "EGF pathway." EGF activates a signaling pathway leading to increased TRPM6 plasma membrane expression and, hence, more Mg^{2+} reabsorption (44). Interestingly, "bone mineralization" was also among the enriched GO terms in mice fed a low-Mg^{2+}-diet. Mg^{2+} plays an important role in this latter process (38). The most evidently enriched functional pathways were observed in high-Mg^{2+} diet-fed mice. Among the upregulated functions, many GO terms indicating mitochondrial activity were evidenced.

DISCUSSION

In this study, the Mg^{2+}-sensitive transcriptome of the DCT was elucidated. By taking advantage of the COPAS sorting system, we were the first to isolate primary DCT material with high purity for gene expression analysis. As a result of our approach, new promising candidate players in renal Mg^{2+} homeostasis were identified. Among the candidates, *1*) SLC41A3 has been proposed as a potential Na^+/Mg^{2+}-exchanging mechanism, *2*) PCBD1 might influence HNF-1β activity, *3*) TBC1D4 is a possible regulator of ion channel membrane availability, and *4*) UMOD could regulate Mg^{2+} transport by decreasing the urinary flow rate.

We isolated DCT cells from mouse kidneys combining the COPAS sorting system with PV-eGFP mice. Until now, it has been difficult to obtain high-quality expression profiles of the isolated DCT fraction because of the quantitative limits of the microdissection technique. Therefore, previously reported expression analyses resulted in a gene expression profile of the combined DCT and CNT (Connecting Tubule) fraction (33). The COPAS system provides the only high-efficiency and high-quality alternative for microdissection. The purity of the COPAS-sorted DCT cells was significantly higher than in previous reports, as demonstrated by the impressive fold enrichments of 200 and 8 for *Ncc* and *Trpm6* (26). The high abundance of mitochondrial genes in our microarray data set further showed sample purity. In the kidney, DCT cells contain the highest amount of mitochondria (9). Inevitably, COPAS-sorted DCT cells can contain adjacent TAL and CNT cells. Although the TAL marker *Nkcc2* was not significantly enriched compared with total kidney samples, transcripts isolated from COPAS-sorted cells may contain genes expressed in the TAL. More importantly, *Trpv5* expression was upregulated in COPAS-sorted DCT cells, which can be explained by the gradual transition of DCT1, via DCT2, to the CNT region, causing a partial overlap of *Pv* and *Trpv5* expression. Since the aim of our study was to identify Mg^{2+}-sensitive gene transcription, the potential limit of sample purity will not affect the results of the microarray analysis. Altogether, this approach allowed the identification of magnesiotropic DCT genes.

Slc41a3. Slc41a3 is probably the most interesting candidate among the newly identified Mg^{2+}-sensitive DCT genes. SLC41A3 is part of a family of three putative Mg^{2+} transporters that were first described by Quamme et al. (34) Using the oocyte voltage-clamp model, it has been shown that all three SLC41 proteins transport Mg^{2+} within its physiological range, although these findings have never been repeated in mammalian cell models (19, 34). SLC41A3 has never been investigated in detail, but lessons from the other SLC41 family members have demonstrated that it consists of 11 transmembrane domains (24). A recent report (20) claimed that

Downloaded from http://ajprenal.physiology.org/ by 10.220.33.6 on October 20, 2016

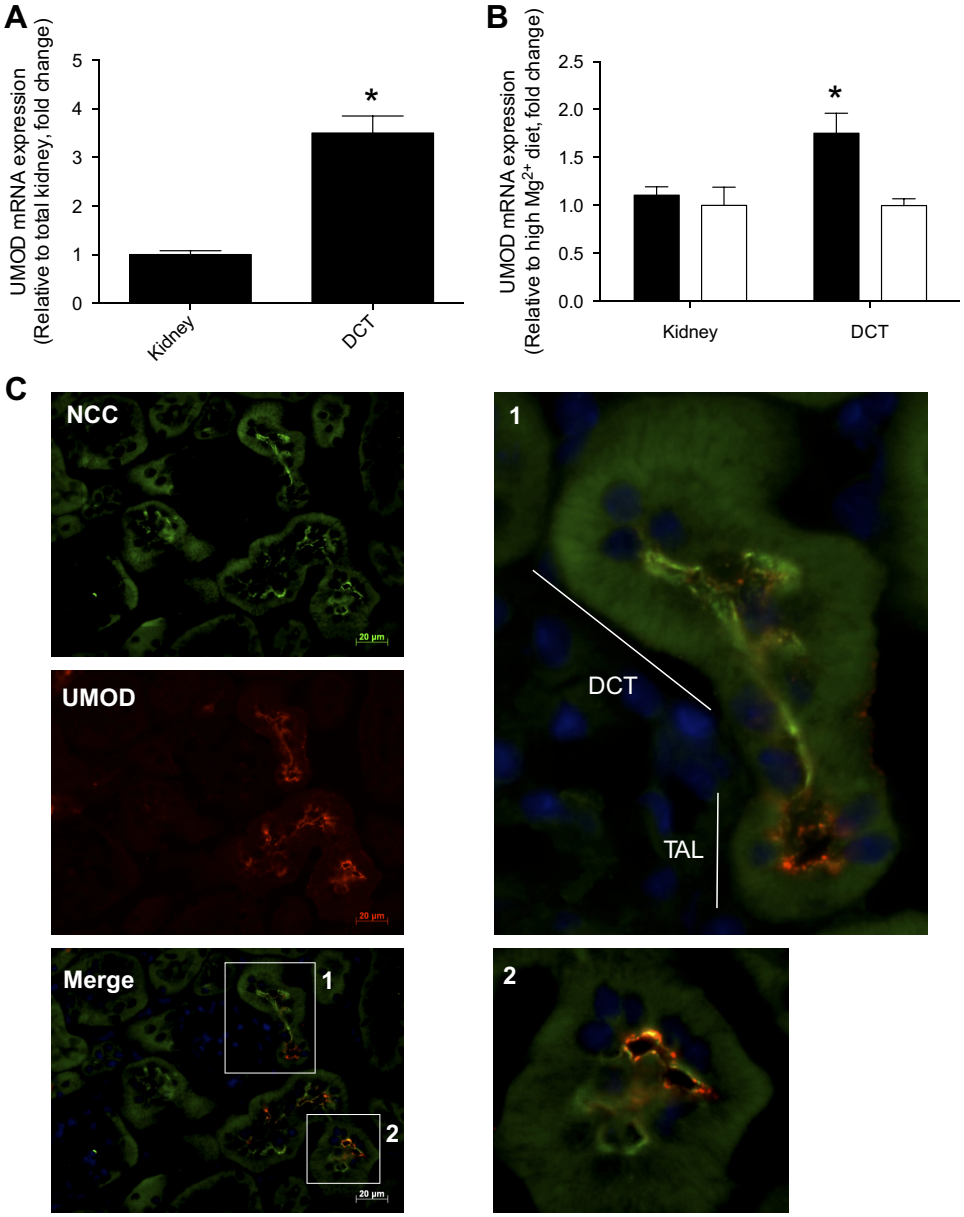

Fig. 5. Expression of Umod in DCTs. *A*: mRNA expression levels of *Umod* in COPAS-selected mouse DCT and control (none selected) kidney tubules were measured by quantitative RT-PCR and normalized for Gapdh expression. Data represent means ± SE and are expressed as fold differences compared with expression in none-selected tubules; $n = 8$. $*P < 0.05$ indicates a significant difference from none-selected tubules. *B*: mRNA expression levels of *Umod* in COPAS-selected DCT tubules and control (none-selected) kidney tubules of mice fed a low or high Mg^{2+}-containing diet were measured by quantitative RT-PCR and normalized for *Gapdh* expression. Data represent means ± SE and are expressed fold differences compared with expression in the high-Mg^{2+} group; $n = 8$. $*P < 0.05$ indicates a significant difference from the high-Mg^{2+} group. *C*: double immunofluorescence staining of mouse kidney sections for NCC (green) and UMOD (red). TAL, thick ascending limb of Henle's loop. Bars = 20 μm.

SLC41A1 could act as a Na^+/Mg^{2+} exchanger. Likewise, the highly homologous SLC41A3 protein could have a similar function. Since SLC41A1 and SLC41A2 are not differentially regulated in the DCT, it seems possible that SLC41A3 is the DCT-specific Mg^{2+} extrusion mechanism. Further research characterizing the function of SLC41A3 is needed to confirm this hypothesis.

Pcbd1. Interestingly, the expression of *Hnf1b* and *Fxyd2* was not differentially regulated in this study. Nevertheless, we identified in *Pcbd1* a potential modulator of HNF-1β/FXYD2 activity. First described in 1991, PCBD1 is a protein with dual activity (28). PCBD1 can stimulate HNF-1α and HNF-1β transcription and has a role in tetrahydrobiopterin regeneration (42). HNF-1 transcriptional activation by PCBD1 does not depend on its enzymatic activity (17). Its role in HNF-1β activation seems of special interest with respect to Mg^{2+} homeostasis. HNF-1β is a transcription factor that stimulates FXYD2 expression, encoding the γ-subunit of Na^+-K^+-ATPase (11). PCBD1, also known as dimerization cofactor of HNF-1 (DCOH), stabilizes the HNF-1 dimer formation necessary for *Fxyd2* transcription. Although PCBD1 activation has never been linked to FXYD2 directly, PCBD1 could indirectly stimulate *Fxyd2* transcription by enhancing HNF-1β function. Given that *Pcbd1* is transcriptionally upregulated in Mg^{2+}-deficient conditions and that such regulation is absent for *Fxyd2* and *Hnf1b*, PCBD1 might be the trigger in FXYD2-mediated fine tuning of Mg^{2+} reabsorption in the DCT.

Tbc1d4. During analyses of the microarray data, another modulator of Na^+-K^+-ATPase activity caught attention. *Tbc1d4*, previously known as AS160, was significantly upregulated in low-Mg^{2+} diet-fed mice. TBC1D4 has been described as a Rab-GTPase-activating kinase involved in the regulation of Na^+-K^+-ATPase plasma membrane availability (2). In this ability, it might directly influence the transmembrane potential that is necessary for Mg^{2+} reabsorption. Interestingly, the function of TBC1D4 is not limited to the regulation of Na^+-

Downloaded from http://ajprenal.physiology.org/ by 10.220.33.6 on October 20, 2016

Table 4. *GO term enrichment analysis of Mg^{2+}-sensitive expression in the DCT*

GO Term	Description	*P* Value	Mean Difference
GO:0060009	Sertoli cell development	0.0004	−0.26
GO:0061036	Positive regulation of cartilage development	0.0002	−0.26
GO:0030238	Male sex determination	0.0018	−0.25
GO:0060170	Cilium membrane	$2.4e^{-5}$	−0.25
GO:0002237	Response to molecule of bacterial origin	0.0043	−0.23
GO:0001158	Enhancer sequence-specific DNA binding	0.0015	−0.22
GO:0030502	Negative regulation of bone mineralization	0.0056	−0.21
GO:0016585	Chromatin remodeling complex	0.0001	−0.20
GO:0043536	Positive regulation of blood vessel endothelial cell migration	0.0065	−0.20
GO:0030903	Notochord development	0.0053	−0.20
GO:0007173	EGF receptor signaling pathway	0.0011	−0.18
GO:0032331	Negative regulation of chondrocyte differentiation	$4.2e^{-7}$	−0.17
GO:0006107	Oxaloacetate metabolic process	0.0059	−0.17
GO:0030279	Negative regulation of ossification	0.0001	−0.16
GO:0010634	Positive regulation of epithelial cell migration	$9.5e^{-6}$	−0.15
GO:0045732	Positive regulation of protein catabolic process	0.0090	−0.14
GO:0071347	Cellular response to interleukin-1	0.0010	−0.13
GO:0016614	Oxidoreductase activity, acting on the CH-OH group of donors	0.0054	−0.13
GO:0035924	Cellular response to vascular endothelial growth factor stimulus	0.0075	−0.11
GO:0005840	Ribosome	$2.3e^{-20}$	0.10
GO:0003735	Structural constituent of the ribosome	$9.4e^{-20}$	0.10
GO:0006694	Steroid biosynthetic process	0.0001	0.11
GO:0022627	Cytosolic small ribosomal subunit	0.0007	0.12
GO:0022900	Electron transport chain	$7.7e^{-14}$	0.14
GO:0005903	Brush border	0.0010	0.14
GO:0006637	Acyl-CoA metabolic process	0.0032	0.16
GO:0005762	Mitochondrial large ribosomal subunit	$1.1e^{-5}$	0.18
GO:0005747	Mitochondrial respiratory chain complex I	$2.4e^{-12}$	0.20
GO:0070469	Respiratory chain	$3.7e^{-19}$	0.21
GO:0008137	NADH dehydrogenase (ubiquinone) activity	$5.3e^{-10}$	0.23
GO:0015238	Drug transmembrane transporter activity	0.0003	0.23
GO:0015893	Drug transport	0.0035	0.24
GO:0003954	NADH dehydrogenase activity	0.0004	0.24
GO:0035634	Response to stilbenoid	0.0002	0.26
GO:0016651	Oxidoreductase activity, acting on NADH or NADPH	$6.7e^{-6}$	0.28

Shown is a summary of the significantly differentially expressed Gene Ontology (GO) terms in the DCT of mice fed a high- or low-Mg^{2+} diet with a minimal difference of 0.1. GO term enrichment was determined by gene set enrichment analysis of the microarray expression data from mRNA specifically isolated from DCT material.

K^+-ATPase. Originally described as a regulator of glucose transporter 4 (GLUT4), TBC1D4 has recently been linked to the regulation of channels including AQP2 and the epithelial Na^{2+} channel (18, 22, 30). Thus, it might be relevant to consider TBC1D4 as a modulator of TRPM6 plasma membrane trafficking. This notion is further supported by the fact that a phosphatidylinositol 3-kinase (PI3K)/Akt/Rac1-mediated pathway activated upon EGF stimulation regulates TRPM6 plasma membrane abundance and that TBC1D4 is an Akt substrate that can also be stimulated by EGF (12, 44). GO term enrichment analysis of our microarray results showed that the EGF pathway was upregulated in low-Mg^{2+} diet-fed mice.

Umod. Although previously implicated in renal ion homeostasis, our finding that *Umod* expression is highly Mg^{2+} sensitive is unprecedented (31). Umod, also described as Tamm-Horshfall glycoprotein, is the most abundant protein in urine, but its exact function remains to be determined (8). It has been proposed that after excretion in the pro-urine, Umod forms an anionic gel-like structure that retards the flow of positively charged ions (46). Increasing *Umod* expression would then decrease the urinary flow rate and thereby enhance the uptake of cations, such as Mg^{2+}. Although often used as a marker for the TAL, *Umod* expression has been described to be not exclusively restricted to the TAL but also to be profound in the early DCT (33, 41). Studies using gene expression microarrays of microdissected DCT tubules were inconclusive. Whereas Pradervand and colleagues (33) showed clear enrichment of *Umod* mRNA expression, another study (5) detected barely any *Umod* mRNA transcripts in the DCT. Immunohistological stainings confirmed the colocalization of UMOD with the DCT marker NCC, although it cannot be excluded that TAL-cleaved UMOD reached the DCT by urinary flow and stuck to the luminal membranes. Interestingly, RT-PCR analysis showed that only DCT expression of *Umod* was Mg^{2+} sensitive, in contrast to *Umod* expression in total kidney samples. This suggests different functional roles of UMOD in DCT and TAL segments of the kidney.

Genes linked to hypomagnesemia. Of all genes that have been linked to hypomagnesemia in human genetic diseases, only a few are transcriptionally regulated (6). *Trpm6*, *Egf*, and *Cnnm2* were modulated, indicating that Mg^{2+} transport is partially regulated at the transcriptional level. Major regulatory pathways are executed on the protein level. The EGF signaling pathway is one of the best-described regulatory mechanisms of TRPM6-mediated Mg^{2+} transport in the DCT (16, 44). Although its mean effectors, such as PI3K, Akt, and Rac1, are not transcriptionally affected by alterations in dietary Mg^{2+} availability, EGF is among the enriched GO terms. Futhermore, *Kcna1*, which codes for the K^+ channel Kv1.1, could not be detected in mouse DCT material by RT-PCR. *Kcna1* is part of a larger family of voltage-gated K^+ channels that are known to form heteromeric complexes. Although Kv1.1 has been implicated in Mg^{2+} handling in patients, its function might be compensated for by other K^+ channels in the PV-eGFP mouse model (14). In this context, it is interesting to note that ROMK is 1.7-fold upregulated in low-Mg^{2+} diet-fed mice. Although this result does not reach statistical significance ($P = 0.06$), it suggests that ROMK might play a role in the maintenance of the luminal membrane potential necessary for Mg^{2+} reabsorption in the DCT.

Ca^{2+}-controlled genes. Inevitably, although changing only dietary Mg^{2+} availability, our approach also led to the detection of many Ca^{2+} homeostasis-related genes, such as the vitamin D receptor, klotho, and calbindin-D28K (35). Activation of the Ca^{2+}-sensing receptor (CaSR) is hypothesized to explain this phenomenon (10). The CaSR is not only sensitive to Ca^{2+} but is also activated upon Mg^{2+} binding. As a result, changes in the availability of Mg^{2+} activate Ca^{2+}-regulatory

Downloaded from http://ajprenal.physiology.org/ by 10.220.33.6 on October 20, 2016

pathways at the local and whole body levels. Hypomagnesemia is, therefore, often associated with a disturbed Ca^{2+} balance in patients (39, 47). In a similar fashion, dietary Mg^{2+} availability influenced Ca^{2+} homeostasis in our mice, as evidenced by the altered serum and urinary Ca^{2+} levels in the present and previous studies (15). Therefore, differential gene expression induced by dietary Mg^{2+} should be analyzed with care. Although serum Ca^{2+} and Mg^{2+} measurements showed that the alterations in Mg^{2+} balance are more profound, it has to be taken into account that differential gene expression might be the effect of Ca^{2+} alterations. The interlink between Ca^{2+} and Mg^{2+} homeostasis was further evidenced in the GO term analysis of the microarray data. Although analyzed in renal samples, bone mineralization was among the enriched GO terms. This might be explained by the fact that many genes involved in renal mineral homeostasis play similar roles in bone formation (6, 38, 44). In addition, GO term analysis identified the upregulation of mitochondrial genes in mice fed the Mg^{2+}-rich diet. This could be a response to an increased intracellular Mg^{2+} concentration in these mice. Intracellular Mg^{2+} is an important ATP-binding factor. Therefore, high Mg^{2+} concentrations in the cell could result in a low unbound ATP availability. Mitochondrial activation will lead to increased ATP production and thereby compensate for the Mg^{2+} binding.

In conclusion, gene expression microarray analysis on primary DCT cells allowed the identification of ample Mg^{2+}-sensitive genes of the mouse genome. Particularly, SLC41A3, PCBD1, TBC1D4, and Umod are candidates that require further investigation. We suggest that patients suffering from hereditary hypomagnesemia of unknown cause be screened for mutations in these candidate genes. The COPAS sorting system provides an excellent mechanism to obtain primary DCT cells. Establishing COPAS-sorted DCT monolayers have been proven to be an accurate method to study thiazide-sensitive Na^+ transport (26, 36). By the use of stable Mg^{2+} isotopes, such as $^{25}Mg^{2+}$ and $^{26}Mg^{2+}$, this primary DCT culture could provide a unique model to examine DCT-specific Mg^{2+} transport. Furthermore, crossbreeding of PV-eGFP mice with the available knockout mouse models, including TRPM6 and NCC knockout mice, further expands the possibilities of the established procedure. This will, in particular, further substantiate the physiological importance of the studied target molecule (6, 48).

ACKNOWLEDGMENTS

The authors thank AnneMiete van der Kemp, Judy Lin, Maikel School, Anke Lameris, Ellen van Loon, and Fariza Bouallala for technical support. Furthermore, Dr. Hannah Monyer (University of Heidelberg) kindly donated the PV-eGFP mice. The authors are grateful to Dr. Nicolas Markadieu and Dr. Titia Woudenberg-Vrenken for optimizing the COPAS sorting system for PV-eGFP tubule sorting and to Dr. Sjoerd Verkaart for critical reading of the manuscript.

GRANTS

This work was supported by The Netherlands Organization for Scientific Research Grants ZonMw 9120.8026 and NWO ALW 818.02.001, Vici Grant NWO-ZonMw 016.130.668 (to J. Hoenderop), and European Union Seventh Framework Programme Grant FP7/2007-2013 (agreement no. 305608).

DISCLOSURES

No conflicts of interest, financial or otherwise, are declared by the author(s).

AUTHOR CONTRIBUTIONS

Author contributions: J.H.d.B., F.C.H., R.J.B., and J.G.H. conception and design of research; J.H.d.B., M.J.G.K., M.L., F.v.Z., and H.M. performed experiments; J.H.d.B. and M.J.G.K. analyzed data; J.H.d.B., F.C.H., R.J.B., and J.G.H. interpreted results of experiments; J.H.d.B., R.J.B., and J.G.H. prepared figures; J.H.d.B. drafted manuscript; J.H.d.B., F.C.H., R.J.B., and J.G.H. edited and revised manuscript; J.H.d.B., R.J.B., and J.G.H. approved final version of manuscript.

REFERENCES

1. **Adalat S, Woolf AS, Johnstone KA, Wirsing A, Harries LW, Long DA, Hennekam RC, Ledermann SE, Rees L, van't Hoff W, Marks SD, Trompeter RS, Tullus K, Winyard PJ, Cansick J, Mushtaq I, Dhillon HK, Bingham C, Edghill EL, Shroff R, Stanescu H, Ryffel GU, Ellard S, Bockenhauer D.** HNF1B mutations associate with hypomagnesemia and renal magnesium wasting. *J Am Soc Nephrol* 20: 1123–1131, 2009.
2. **Alves DS, Farr GA, Seo-Mayer P, Caplan MJ.** AS160 associates with the Na^+,K^+-ATPase and mediates the adenosine monophosphate-stimulated protein kinase-dependent regulation of sodium pump surface expression. *Mol Biol Cell* 21: 4400–4408, 2010.
3. **Belge H, Gailly P, Schwaller B, Loffing J, Debaix H, Riveira-Munoz E, Beauwens R, Devogelaer JP, Hoenderop JG, Bindels RJ, Devuyst O.** Renal expression of parvalbumin is critical for NaCl handling and response to diuretics. *Proc Natl Acad Sci USA* 104: 14849–14854, 2007.
4. **Bockenhauer D, Feather S, Stanescu HC, Bandulik S, Zdebik AA, Reichold M, Tobin J, Lieberer E, Sterner C, Landoure G, Arora R, Sirimanna T, Thompson D, Cross JH, van't Hoff W, Al Masri O, Tullus K, Yeung S, Anikster Y, Klootwijk E, Hubank M, Dillon MJ, Heitzmann D, Arcos-Burgos M, Knepper MA, Dobbie A, Gahl WA, Warth R, Sheridan E, Kleta R.** Epilepsy, ataxia, sensorineural deafness, tubulopathy, and KCNJ10 mutations. *N Engl J Med* 360: 1960–1970, 2009.
5. **Cheval L, Pierrat F, Dossat C, Genete M, Imbert-Teboul M, Duong Van Huyen JP, Poulain J, Wincker P, Weissenbach J, Piquemal D, Doucet A.** Atlas of gene expression in the mouse kidney: new features of glomerular parietal cells. *Physiol Genomics* 43: 161–173, 2011.
6. **de Baaij JH, Hoenderop JG, Bindels RJ.** Regulation of magnesium balance: lessons learned from human genetic disease. *Clin Kidney J* 5: i14–i24, 2012.
7. **de Baaij JH, Stuiver M, Meij IC, Lainez S, Kopplin K, Venselaar H, Muller D, Bindels RJ, Hoenderop JG.** Membrane topology and intracellular processing of cyclin M2 (CNNM2). *J Biol Chem* 287: 13644–13655, 2012.
8. **Devuyst O, Dahan K, Pirson Y.** Tamm-Horsfall protein or uromodulin: new ideas about an old molecule. *Nephrol Dial Transplant* 20: 1290–1294, 2005.
9. **Dørup J.** Ultrastructure of distal nephron cells in rat renal cortex. *J Ultrastruct Res* 92: 101–118, 1985.
10. **Ferre S, Hoenderop JG, Bindels RJ.** Sensing mechanisms involved in Ca^{2+} and Mg^{2+} homeostasis. *Kidney Int* 82: 1157–1166, 2012.
11. **Ferre S, Veenstra GJ, Bouwmeester R, Hoenderop JG, Bindels RJ.** HNF-1B specifically regulates the transcription of the γa-subunit of the Na^+/K^+-ATPase. *Biochem Biophys Res Commun* 404: 284–290, 2011.
12. **Geraghty KM, Chen S, Harthill JE, Ibrahim AF, Toth R, Morrice NA, Vandermoere F, Moorhead GB, Hardie DG, MacKintosh C.** Regulation of multisite phosphorylation and 14-3-3 binding of AS160 in response to IGF-1, EGF, PMA and AICAR. *Biochem J* 407: 231–241, 2007.
13. **Gkika D, Mahieu F, Nilius B, Hoenderop JG, Bindels RJ.** 80K-H as a new Ca^{2+} sensor regulating the activity of the epithelial Ca^{2+} channel transient receptor potential cation channel V5 (TRPV5). *J Biol Chem* 279: 26351–26357, 2004.
14. **Glaudemans B, van der Wijst J, Scola RH, Lorenzoni PJ, Heister A, van der Kemp AW, Knoers NV, Hoenderop JG, Bindels RJ.** A missense mutation in the Kv1.1 voltage-gated potassium channel-encoding gene KCNA1 is linked to human autosomal dominant hypomagnesemia. *J Clin Invest* 119: 936–942, 2009.
15. **Groenestege WM, Hoenderop JG, van den Heuvel L, Knoers N, Bindels RJ.** The epithelial Mg^{2+} channel transient receptor potential melastatin 6 is regulated by dietary Mg^{2+} content and estrogens. *J Am Soc Nephrol* 17: 1035–1043, 2006.
16. **Groenestege WM, Thebault S, van der Wijst J, van den Berg D, Janssen R, Tejpar S, van den Heuvel LP, van Cutsem E, Hoenderop JG, Knoers NV, Bindels RJ.** Impaired basolateral sorting of pro-EGF

Downloaded from http://ajprenal.physiology.org/ by 10.220.33.6 on October 20, 2016

causes isolated recessive renal hypomagnesemia. *J Clin Invest* 117: 2260–2267, 2007.
17. **Johnen G, Kaufman S.** Studies on the enzymatic and transcriptional activity of the dimerization cofactor for hepatocyte nuclear factor 1. *Proc Natl Acad Sci USA* 94: 13469–13474, 1997.
18. **Kim HY, Choi HJ, Lim JS, Park EJ, Jung HJ, Lee YJ, Kim SY, Kwon TH.** Emerging role of Akt substrate protein AS160 in the regulation of AQP2 translocation. *Am J Physiol Renal Physiol* 301: F151–F161, 2011.
19. **Kolisek M, Launay P, Beck A, Sponder G, Serafini N, Brenkus M, Froschauer EM, Martens H, Fleig A, Schweigel M.** SLC41A1 is a novel mammalian Mg^{2+} carrier. *J Biol Chem* 283: 16235–16247, 2008.
20. **Kolisek M, Nestler A, Vormann J, Schweigel-Rontgen M.** Human gene *SLC41A1* encodes for the Na^+/Mg^{2+} exchanger. *Am J Physiol Cell Physiol* 302: C318–C326, 2012.
21. **Lameris AL, Monnens LA, Bindels RJ, Hoenderop JG.** Drug-induced alterations in Mg^{2+} homoeostasis. *Clin Sci (Lond)* 123: 1–14, 2012.
22. **Liang X, Butterworth MB, Peters KW, Frizzell RA.** AS160 modulates aldosterone-stimulated epithelial sodium channel forward trafficking. *Mol Biol Cell* 21: 2024–2033, 2010.
23. **Limaye CS, Londhey VA, Nadkart MY, Borges NE.** Hypomagnesemia in critically ill medical patients. *J Assoc Physicians India* 59: 19–22, 2011.
24. **Mandt T, Song Y, Scharenberg AM, Sahni J.** SLC41A1 Mg^{2+} transport is regulated via Mg^{2+}-dependent endosomal recycling through its N-terminal cytoplasmic domain. *Biochem J* 439: 129–139, 2011.
25. **Margaritis T, Lijnzaad P, van Leenen D, Bouwmeester D, Kemmeren P, van Hooff SR, Holstege FC.** Adaptable gene-specific dye bias correction for two-channel DNA microarrays. *Mol Syst Biol* 5: 266, 2009.
26. **Markadieu N, San-Cristobal P, Nair AV, Verkaart S, Lenssen E, Tudpor K, van Zeeland F, Loffing J, Bindels RJ, Hoenderop JG.** A primary culture of distal convoluted tubules expressing functional thiazide-sensitive NaCl transport. *Am J Physiol Renal Physiol* 303: F886–F892, 2012.
27. **Meij IC, Koenderink JB, van Bokhoven H, Assink KF, Groenestege WT, de Pont JJ, Bindels RJ, Monnens LA, van den Heuvel LP, Knoers NV.** Dominant isolated renal magnesium loss is caused by misrouting of the Na^+,K^+-ATPase γ-subunit. *Nat Genet* 26: 265–266, 2000.
28. **Mendel DB, Khavari PA, Conley PB, Graves MK, Hansen LP, Admon A, Crabtree GR.** Characterization of a cofactor that regulates dimerization of a mammalian homeodomain protein. *Science* 254: 1762–1767, 1991.
29. **Meyer AH, Katona I, Blatow M, Rozov A, Monyer H.** In vivo labeling of parvalbumin-positive interneurons and analysis of electrical coupling in identified neurons. *J Neurosci* 22: 7055–7064, 2002.
30. **Miinea CP, Sano H, Kane S, Sano E, Fukuda M, Peranen J, Lane WS, Lienhard GE.** AS160, the Akt substrate regulating GLUT4 translocation, has a functional Rab GTPase-activating protein domain. *Biochem J* 391: 87–93, 2005.
31. **Mutig K, Kahl T, Saritas T, Godes M, Persson P, Bates J, Raffi H, Rampoldi L, Uchida S, Hille C, Dosche C, Kumar S, Castaneda-Bueno M, Gamba G, Bachmann S.** Activation of the bumetanide-sensitive $Na^+,K^+,2Cl^-$ cotransporter (NKCC2) is facilitated by Tamm-Horsfall protein in a chloride-sensitive manner. *J Biol Chem* 286: 30200–30210, 2011.
32. **Nijenhuis T, Hoenderop JG, Loffing J, van der Kemp AW, van Os CH, Bindels RJ.** Thiazide-induced hypocalciuria is accompanied by a decreased expression of Ca^{2+} transport proteins in kidney. *Kidney Int* 64: 555–564, 2003.
33. **Pradervand S, Zuber Mercier A, Centeno G, Bonny O, Firsov D.** A comprehensive analysis of gene expression profiles in distal parts of the mouse renal tubule. *Pflügers Arch* 460: 925–952, 2010.
34. **Quamme GA.** Molecular identification of ancient and modern mammalian magnesium transporters. *Am J Physiol Cell Physiol* 298: C407–C429, 2010.
35. **Renkema KY, Nijenhuis T, van der Eerden BC, van der Kemp AW, Weinans H, van Leeuwen JP, Bindels RJ, Hoenderop JG.** Hypervitaminosis D mediates compensatory Ca^{2+} hyperabsorption in TRPV5 knockout mice. *J Am Soc Nephrol* 16: 3188–3195, 2005.
36. **Riveira-Munoz E, Chang Q, Godefroid N, Hoenderop JG, Bindels RJ, Dahan K, Devuyst O.** Transcriptional and functional analyses of SLC12A3 mutations: new clues for the pathogenesis of Gitelman syndrome. *J Am Soc Nephrol* 18: 1271–1283, 2007.
37. **Roepman P, de Koning E, van Leenen D, de Weger RA, Kummer JA, Slootweg PJ, Holstege FC.** Dissection of a metastatic gene expression signature into distinct components. *Genome Biol* 7: R117, 2006.
38. **Rude RK, Gruber HE.** Magnesium deficiency and osteoporosis: animal and human observations. *J Nutr Biochem* 15: 710–716, 2004.
39. **Schlingmann KP, Weber S, Peters M, Niemann Nejsum L, Vitzthum H, Klingel K, Kratz M, Haddad E, Ristoff E, Dinour D, Syrrou M, Nielsen S, Sassen M, Waldegger S, Seyberth HW, Konrad M.** Hypomagnesemia with secondary hypocalcemia is caused by mutations in TRPM6, a new member of the TRPM gene family. *Nat Genet* 31: 166–170, 2002.
40. **Sedlacek M, Schoolwerth AC, Remillard BD.** Electrolyte disturbances in the intensive care unit. *Semin Dial* 19: 496–501, 2006.
41. **Sikri KL, Foster CL, MacHugh N, Marshall RD.** Localization of Tamm-Horsfall glycoprotein in the human kidney using immuno-fluorescence and immuno-electron microscopical techniques. *J Anat* 132: 597–605, 1981.
42. **Sourdive DJ, Transy C, Garbay S, Yaniv M.** The bifunctional DCOH protein binds to HNF1 independently of its 4-α-carbinolamine dehydratase activity. *Nucleic Acids Res* 25: 1476–1484, 1997.
43. **Stuiver M, Lainez S, Will C, Terryn S, Gunzel D, Debaix H, Sommer K, Kopplin K, Thumfart J, Kampik NB, Querfeld U, Willnow TE, Nemec V, Wagner CA, Hoenderop JG, Devuyst O, Knoers NV, Bindels RJ, Meij IC, Muller D.** CNNM2, encoding a basolateral protein required for renal Mg^{2+} handling, is mutated in dominant hypomagnesemia. *Am J Hum Genet* 88: 333–343, 2011.
44. **Thebault S, Alexander RT, Tiel Groenestege WM, Hoenderop JG, Bindels RJ.** EGF increases TRPM6 activity and surface expression. *J Am Soc Nephrol* 20: 78–85, 2009.
45. **van de Peppel J, Kemmeren P, van Bakel H, Radonjic M, van Leenen D, Holstege FC.** Monitoring global messenger RNA changes in externally controlled microarray experiments. *EMBO Rep* 4: 387–393, 2003.
46. **Vyletal P, Bleyer AJ, Kmoch S.** Uromodulin biology and pathophysiology–an update. *Kidney Blood Press Res* 33: 456–475, 2010.
47. **Walder RY, Landau D, Meyer P, Shalev H, Tsolia M, Borochowitz Z, Boettger MB, Beck GE, Englehardt RK, Carmi R, Sheffield VC.** Mutation of TRPM6 causes familial hypomagnesemia with secondary hypocalcemia. *Nat Genet* 31: 171–174, 2002.
48. **Woudenberg-Vrenken TE, Sukinta A, van der Kemp AW, Bindels RJ, Hoenderop JG.** Transient receptor potential melastatin 6 knockout mice are lethal whereas heterozygous deletion results in mild hypomagnesemia. *Nephron Physiol* 117: p11–19, 2011.
49. **Wu H, Kerr MK, Cui X, Churchill GA.** MAANOVA: a software package for the analysis of spotted cDNA microarray experiments. In: *The Analysis of Gene Expression Data: Methods and Software*. New York: Springer, 2012, p. 313–342.
50. **Yang YH, Dudoit S, Luu P, Lin DM, Peng V, Ngai J, Speed TP.** Normalization for cDNA microarray data: a robust composite method addressing single and multiple slide systematic variation. *Nucleic Acids Res* 30: e15, 2002.

Downloaded from http://ajprenal.physiology.org/ by 10.220.33.6 on October 20, 2016